Received: 26 October 2017 | Revised: 21 December 2017 | Accepted: 7 January 2018 | Published on: 3 July 2018

DOI: 10.1002/ctpp.201700160

ORIGINAL ARTICLE

Contributions to Plasma Physics

Simulation study on the vapour shielding at solid walls under transient heat loads using weighted particle model

K. Ibano[1] | Y. Kikuchi[2] | A. Tanaka[2] | S. Togo[3] | H. T. Lee[1] | Y. Ueda[1] | T. Takizuka[1]

[1]Graduate School of Engineering, Osaka University, Suita, Japan
[2]Graduate School of Engineering, University of Hyogo, Himeji, Japan
[3]Plasma Research Center, University of Tsukuba, Tsukuba, Japan

***Correspondence**
K. Ibano, Graduate school of Engineering, Osaka University, Suita 565-0871, Japan.
Email: kibano@eei.eng.osaka-u.ac.jp

Funding Information
This research was supported by the ZE Research Program, IAE ZE29B-01. NIFS Collaboration Research Program, NIFS16KNXN320.

Vapour shielding at solid walls is expected for a future fusion reactor in case of large heat load due to transient events. In order to estimate the dissipation of the incoming heat flux by the vapour shielding, a simulation code called PIXY, using a weighted particle model, is developed. First, a validation study is undertaken. Vapour shielding of an aluminium-coated tungsten specimen was experimentally observed in a plasma gun device. Results are reproduced by the PIXY simulation. Then, the code is applied to the transient edge-localized mode (ELM) heat flux for the reactor condition. It was found that the ion–neutral collision, as well as radiative cooling, is a dominant phenomenon for the heat flux dissipation in both cases. As the maximum heat flux increases, oscillating phenomena appear remarkably, which have been observed in other experimental studies on vapour shielding.

KEYWORDS
particle-in-cell simulation, plasma–surface interaction, vapour shielding, weighted particle

1 | INTRODUCTION

Interest in vapour shielding is increasing as it is an inherent mitigation of intense heat load to first wall (FW) of plasma-facing components (PFCs).[1–5] Historically, vapour shielding was studied for the pellet injection into the magnetized confined plasma.[6–8] Hydrogen pellets were injected in order to fuel the core plasma. However, these pellets were not absorbed in the core as fast as expected. It was found that the vapour clouds surrounding the pellet shield the incoming plasma heat flux. Now, wall erosion due to transient heat loads in ITER is a large concern.[9] Slow transient (~20 MW/m^2, 10 s), edge-localized mode (ELM) (0.1 ~ 1 GW/m^2, 0.1 ~ 1 ms), and disruption (1 ~ 10 GW/m^2, a few ms) cause erosions on the surface of PFCs. In case vapour shielding occurs, lower amounts of heat loads are absorbed into the wall. Thus, vapour shielding can be an inherent relief for the intense heat flux. During vapour shielding at a solid wall, several physical phenomena occur simultaneously. Melting of the solid surface due to intense thermal loads, molten layer instability on the surface, droplet ejections, and vapour emission and their ionization cause multiphase matters, that is, plasma, gas, liquid, and solid phases. In addition to these multiphase interactions, plasma–surface interactions cause secondary electron emissions, recycling of ions as neutrals, reflection, sputtering, and so on. Ejected particles get ionized, and some parts of them return to the surface through the sheath potential or the gyro motion and are re-deposited promptly. Incoming plasma heat loads can be dissipated by Coulomb collision, ion–neutral collision, and radiative excitation with these wall-originated impurities. These reactions are summarized in a schematic image in Figure 1. In order to examine the effects of these reactions, analytical modelling[10] and simulation studies[11,12] have been carried out. Most of these simulation studies were based on the fluid model. In the fluid model, the boundary conditions are usually set on a plasma sheath entrance. However, vapour shielding occurs mainly in the vicinity of an FW, and the reactions in the sheath region should be solved. Thus, we employ a Particle-In-Cell (PIC) simulation for this sake. The simulation model is briefly described in the next section. The aims of this study are understandings and predictions on vapour shielding under transient heat loads at the reactor conditions. In order to validate our simulation code beforehand, a comparison was made with interactions between linear-plasma and laser-ablated vapour.[13] Here, we make another comparison with experimental observations of vapour shielding in a plasma gun (PG). An Al-coated W specimen was irradiated by helium plasma. Al was used

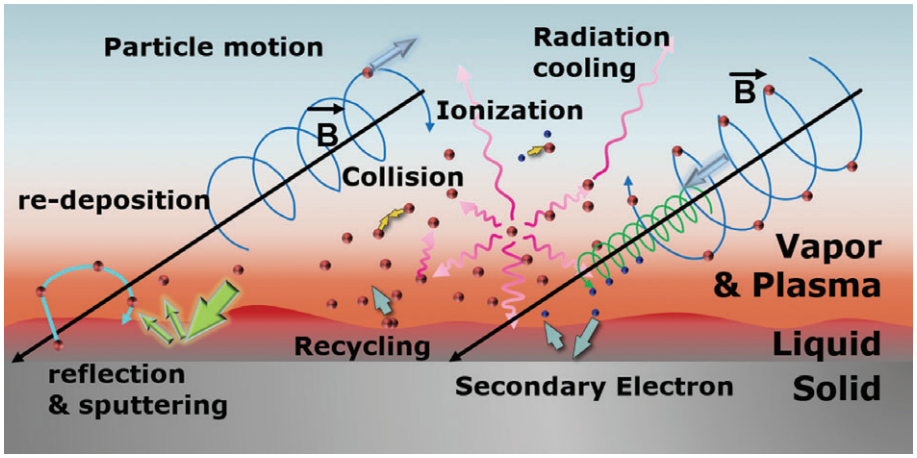

FIGURE 1 Schematic image of the multi-phase interaction during the transient heat load at a solid wall

as a mimic of Be, as used in the ITER first wall. W divertor tiles are assumed to be deposited by FW-originated Be. Heat flux dissipation in the PG was observed for the Al-coated W specimen due to the expanding Al clouds. Present PIC simulation is applied to reproduce the experimental observation (Section 3.2). Then, the simulation code is also applied for the ELM in a reactor condition (Section 3.3).

2 | MODEL DESCRIPTION

2.1 | 1d3v PIC and 1d heat transfer model

In the vapour shielding simulation, plasma behaviour in the vicinity of walls is important. Thus, we developed a PIC code, named PIXY, and applied it to the simulation.[13,14] The PIXY code solves trajectories of all particles for one dimension in space and three dimensions in velocity (1d3v). Debye sheath as well as magnetic pre-sheath can be successfully simulated with this coordination. In the 1d simulation space, plasma super particles are supplied at a Langevin heat bath region, which is given as velocity distribution in temperature ($T_e = 100\,\mathrm{eV}$). At the central region of the system, heating was applied by a Langevin heat bath model,[10] which was given as

$$\frac{\Delta}{\Delta t}\mathrm{v}_j = -\nu \mathrm{v}_j + A \tag{1}$$

$$\langle A^2 \rangle = \frac{2T_{L0}}{m_j}\frac{\nu}{\Delta t} \tag{2}$$

where v_j is velocity of a particle, T_{L0} is a specified temperature, m_j is mass of a particle, ν is a relaxation frequency, and A is a random number with uniform distribution. The square mean value of A is given by Equation 2. The super particles leave the heat bath and move towards the boundary of the system. As they reach the boundary, their energy is counted as the heat flux to the wall (or specimen), and sputtering is examined. Then, information of these super particles is initialized, and these particles are re-fuelled into the heat bath in order to maintain the total amount of the particles in the system. An external magnetic field can be applied, and the electromagnetic forces on charged particles are simulated. Direction of the 1d space is normal to the target, and the tilting angle of the magnetic field is given arbitrarily.

In order to simulate ELM or disruption in the magnetic confined device, a two-component plasma model is used. First, ions and electrons of background plasma are fed into the system with a Maxwellian distribution for a specific temperature. As the system becomes a steady-state condition, fast particles corresponding with ELM or disruption plasma are injected. Density and temperature of this plasma are separately calculated. Then, atomic–molecular (A&M) reactions are solved for both plasma and also separately.

Several A&M reactions, ionization, recombination, and line, Bremsstrahlung, and recombination radiations are treated in the code. Monte Carlo techniques are applied to simulate these reactions. Based on their reaction rates in the OPEN-ADAS database,[15] the probabilities of these reactions in a time-step are examined and compared with a random number. When the reaction occurs, corresponding energy balance is maintained by loss or gain of a randomly selected electron in a same cell.

In the radiation model, cooling power is calculated based on the "stage-to-stage" emission coefficients of the OPEN-ADAS library. Ions are assumed to be in their ground states. Although the power of each line cannot be obtained from this model, the total energy loss of electrons is determined. It should be mentioned here that the line radiation trapping is not considered in this study. In the high-density shielding plasma, the trapping is expected to play an important role.[10,16] However, calculations of the radiation transport and trapping are costly. Thus, we tentatively chose a model with transparent plasma. This model does

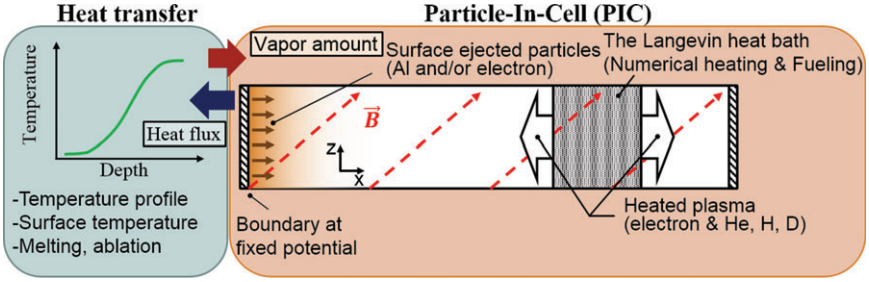

FIGURE 2 Schematic of the calculation model

overly estimate the radiation cooling. Trapped radiation power increases the shielding plasma energy and the ionization rate. However, as discussed in the following section, ion–neutral collisions, the main topic of this study, can work substantially for heat dissipation, even in an optically thick shielding plasma.

The sputtering is simulated using a dataset based on a semi-empirical model.[17] Sputtering coefficient data are summarized as a function of incident energy and angles in numerical tables. When an ion reaches the boundary, its incident energy and angle to the surface is examined, and its sputtering coefficient is determined by a bilinear interpolation from the table. Super particles are ejected from the surface as the sputtered particles and their weights are given using the evaluated sputtering coefficient.

As mentioned above, the heat flux to the walls are counted using the total energy of the super particles reaching the boundary. Then, a heat transfer calculation is performed for the wall component using the heat flux as a surface boundary. The following 1d heat transfer equation is solved:

$$\rho C_p \frac{\partial T}{\partial t} = \frac{\partial}{\partial x}\left(\kappa \frac{\partial T}{\partial x}\right), \tag{3}$$

where ρ, C_p, and κ are density, heat capacity, and thermal conductivity, respectively. A multi-layer model is used in the calculation. No thermal resistivity between layers is assumed. A boundary condition at the plasma side is the heat flux boundary calculated in the PIXY code. A coolant flow or an insulation boundary is assumed for a boundary condition on another side. Based on the calculated surface temperature, the evaporation rates of surface materials are determined. These evaporated particles are fed into the plasma side. The energetic cost of evaporation is taken into account at the surface boundary heat flux. Overall, simulation models are summarized schematically in Figure 2.

2.2 | Weighted particle model

The vapour ejection rate changes significantly with surface temperature. Thus, if same particle weights are used for plasma super particles and impurity super particles, the numbers of super particles in the calculations becomes significantly large. Thus, instead of using same weights for all particles, we use the weighted particle model. In this model, particle weights are different for all super particles to represent the different emission rates of impurity particles. In order to treat A&M reactions for these weighted particles, special attention was paid. For example, in case of radiation cooling from impurity, energy should be extracted from an electron super particle near the impurity. However, in case of radiation cooling from a large weight impurity, one electron super particle cannot provide enough energy for the radiation because of the weight difference. Thus, instead of taking energy from one neighbour electron, multiple electron super particles in the vicinity are chosen, and energy corresponding to the radiation cooling is extracted from them. For the ionization and the recombination reactions, the stick and snatch model in Refs [13, 14] is used.

2.3 | Ion–neutral collision model

Ion–neutral collision is simulated by a Monte Carlo method in a similar fashion as the A&M reactions. Collision of a neutral particle is examined using a comparison between a corresponding reaction rate and a random number. The elastic cross section between H^+ and Be can be found in Ref. [18]. Other ion–neutral elastic cross sections are calculated from the semi-classical approximation explained in Ref. [18], where the dipole polarizability is taken from Ref. [19]. Once reaction is determined, an ion in a same cell is randomly selected. A collision between the selected ion and the corresponding neutral super particle is solved by a binary collision-based model. These super particles generally have different weights. Velocities of a particle a with lighter weight, wa, and a particle b with heavier weight, wb, are scattered by a collision as follows:

$$\mathrm{v}_\mathrm{a}^{t+\Delta t} = \mathrm{v}_\mathrm{a}^{t} + (m_\mathrm{ab}/m_\mathrm{b})\{-\boldsymbol{u}(1-\cos\Theta) + u\boldsymbol{x}_\perp \sin\Theta\} \tag{4}$$

$$\mathrm{v}_\mathrm{b}^{t+\Delta t} = \mathrm{v}_\mathrm{b}^{t} - P(m_\mathrm{ab}/m_\mathrm{b})\{-\boldsymbol{u}(1-\cos\Theta) + u\boldsymbol{x}_\perp \sin\Theta\} \tag{5}$$

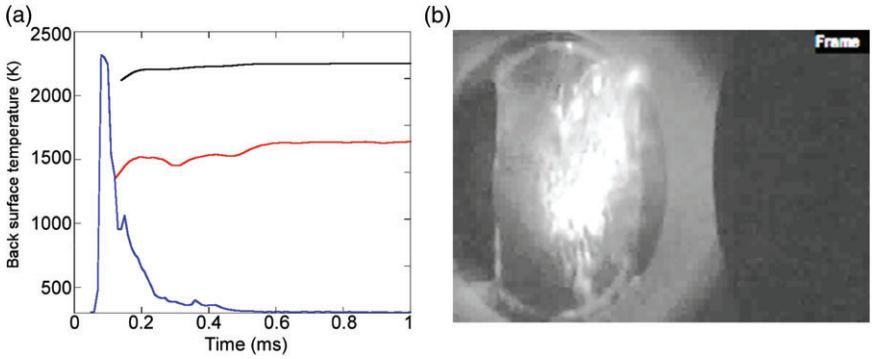

FIGURE 3 (a) Development of back surface temperature during the plasma gun pulse for the plane W and the Al-coated W specimens. (b) An Al band-pass filtered (394 nm) high-speed camera image of the Al-coated W under He irradiation at 100 μs after the plasma pulse begins

$$\boldsymbol{x}_\perp = \left(\frac{u_x u_z}{u_\perp u} \cos\Phi - \frac{u_y}{u_\perp} \sin\Phi, \frac{u_y u_z}{u_\perp u} \cos\Phi + \frac{u_x}{u_\perp} \sin\Phi, -\frac{u_\perp}{u} \cos\Phi \right) \tag{6}$$

where $m_{ab} = m_a\, m_b/(m_a + m_b)$, $\mathbf{u} = \mathbf{v}_a^t - \mathbf{v}_b^t$, and Θ and Φ are the reduced mass, the relative velocity, and scattering angles, respectively. In the Coulomb collision model, Θ is obtained from a random number based on the Coulomb forces. In the ion–neutral collision, Θ is randomly determined from 0 to π. Φ is also a random angle from 0 to 2π. The weight difference is treated by the rejection model. The velocity correction of a heavier-weight particle is taken with a probability of the weight ratio, that is, the probability factor p is unity for a uniform random number less than wa/wb; otherwise, $p = 0$, while the velocity correction of a lighter-weight particle is always taken.

In order to avoid over-counting of these collision effects, neutral particle positions are tracked in a 3d space. Once neutral particles leave a plasma tube, these particles are counted as pumped out. In the PG simulation (Section 3.2), the neutrals are uniformly ejected from a 3 cm diameter specimen, and a 10 cm diameter plasma tube is used as the boundary. In the case of the ELM simulation (Section 3.3), a 1 cm-thick scrape-off-layer plasma and wetted area is assumed.

3 | RESULTS

3.1 | PG experiment

Observation of vapour shielding has been undertaken by irradiating an Al-coated W specimen with a helium PG shot. Electron temperature ($T_e \sim 30$ eV and density ($n_e \sim 10^{21}$ m^{-3}) were achieved. The energy density of 1 MJ/m^2 was irradiated in 0.2 ms. The detail of the PG experiment can be found in refs [20, 21]. With this device, an Al-coated W specimen was irradiated. A thin W specimen with a thickness of 50 μm was coated by an Al thin layer with a thickness of 3 μm. Strong evaporation of Al during irradiation was confirmed by Al I line emissions. Specimen temperature was monitored by a pyrometer on the back surface and plotted in Figure 3a. Steady-state temperatures of the W and Al/W specimens after the shots were 2250 and 1600 K, respectively.

3.2 | Simulation on PG experiment

Figure 4 shows the PG simulation results at different time steps. At the beginning of the PG pulse, temperature and density of plasma gradually develop to 30 eV and 3×10^{21} m^{-3}. Al erosion already begins at this point; thus excitation, recombination, and Bremsstrahlung radiation is observed. Then, as the PG pulse reaches its maximum, massive evaporation of Al due to the ablation begins. Thus, density increases in the vicinity of the wall. Increasing radiation dissipates PG energy, and thus, a temperature drop is also observed. The Al radiation reaches ~1 cm from the target in the simulation. This agrees with the experimental observation shown in Figure 3b in which the peak of the Al radiation is around 5 mm at 100 μs after the pulse. Finally, the Al cloud expands to the entire calculation region. The increased radiation region dissipates the PG plasma energy. Temporal change of the heat flux q" during the pulse is shown in Figure 5a. Surface temperature of Al is also shown in the same figure. Development of heat flux as the PG plasma reaches the steady states is seen until 20 μs after the pulse starts. A strong decrease of heat flux is seen at 100 μs. In contrast, PG heat flux to the W specimen remains constant during the PG pulse. The heat flux dissipation is well seen from this result. However, if we examine the individual heat flux of electrons and ions, it is found that no dissipation occurs in the PG ions if the ion–neutral collisions are not taken into account. The temporal change of the heat flux with the ion–neutral collision model is shown in Figure 6. This temporal change shows the remarkable heat flux dissipation of ions due to ion–neutral collision, which is comparable to the radiation cooling without radiation trapping. Thus, although the radiation transport and trapping models need to be included for the precise heat flux estimation, it can be concluded that the ion–neutral collision is also an important phenomena during the vapour shielding as well as the radiation cooling on electrons.

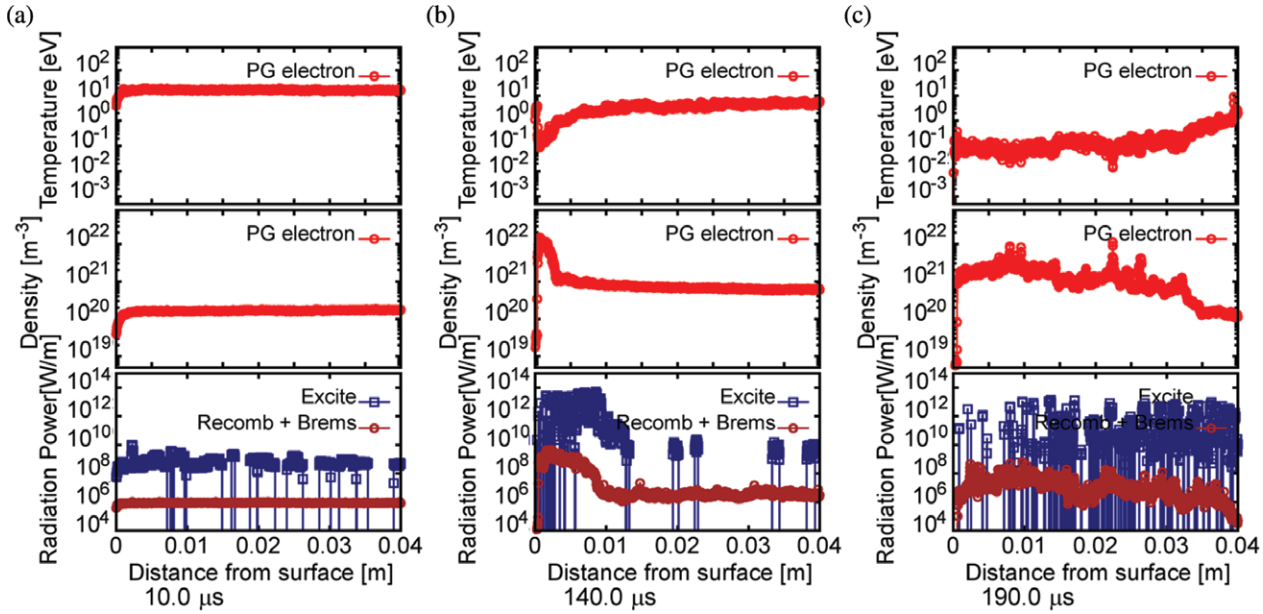

FIGURE 4 Development of density and temperature of plasma gun (PG) electron and radiation power from Al impurities. (a) 10 μs, (b) 140 μs, (c) 190 μs.

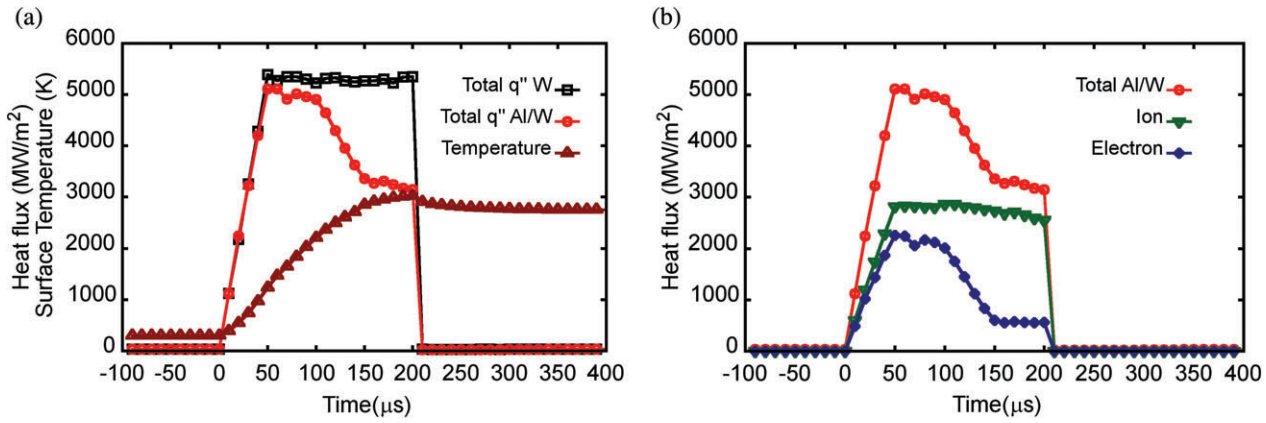

FIGURE 5 (a) Temporal change of heat flux during the plasma gun pulse for the plane W and the Al-coated W specimens. The development of surface temperature for the Al-coated W specimen is also shown. (b) Temporal change of individual heat flux during the plasma gun pulse for the Al-coated W specimen

In this experiment, the back surface temperature reaches 2250 K in the case of the W specimen and 1600 K in the case of the Al/W specimen. However, in the simulation shown in Figure 4, the back surface temperature reaches 3000 K for the W specimen and 2400 K for the Al/W specimen. Thus, the actual absorbed heat flux in the experiments should be lower than the q" ~ 5 GW/m^2. A parametric survey was undertaken and is summarized in Figure 7. It is found that, in the case of a lower heat flux q" ~ 3 GW/m^2, the back surface temperature becomes 2250 K for the W specimen in the simulation. However, in this case, the difference between the W specimen and the Al/W specimen becomes significantly lower than 600 K. The temperature difference corresponds to the heat flux dissipation by the Al vapour. Thus, in case of the calculation with q" ~ 3 GW/m^2, not much Al vapour is generated if the ablation threshold is assumed as the boiling point in the atmosphere (2743 K). In the experiments, the Al droplets are observed in the high-speed camera images. Thus, surface ablation does occur even if the back surface temperature remains steady at ~1600 K. In order to simulate this ablation condition, simulations are repeated with lower ablation threshold values. Then, it is confirmed that the experimental result can be reproduced with simulation with q″ ~ 3 GW/m^2 and the ablation threshold between 1600 and 1800 K, as shown in Figure 7.

3.3 | ELM condition

Vapour shielding of the Be wall under ELM-like flux is simulated. A 6° incident angle of 2 T magnetic field is assumed. A 200 μs plasma pulse with $T_e \sim 2$ keV, $n_e \sim 5 \times 10^{19}$ m^{-3}, and q″ ~ 3 GW/m^2 is simulated. We compare the heat flux of no vapour shielding, energy dissipation via radiation only, and energy dissipation via radiation and ion–neutral collisions as shown in Figure 8. The energy dissipations are also observable for radiation and ion–neutral collisions in this reactor condition calculation.

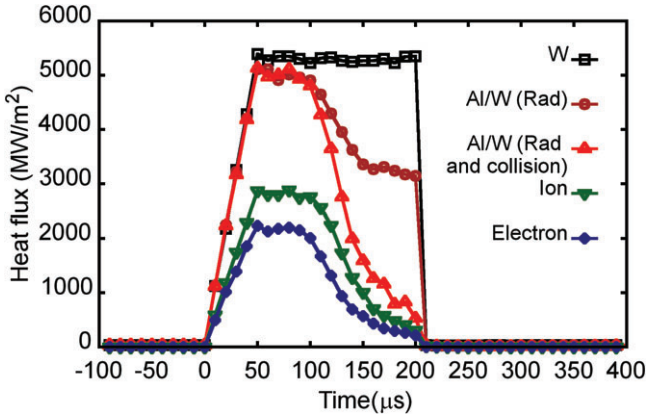

FIGURE 6 Temporal change of heat flux during the plasma gun pulse for the plane W and the Al-coated W specimens. Individual heat flux for the Al-coated W specimen with ion–neutral collision model is also shown

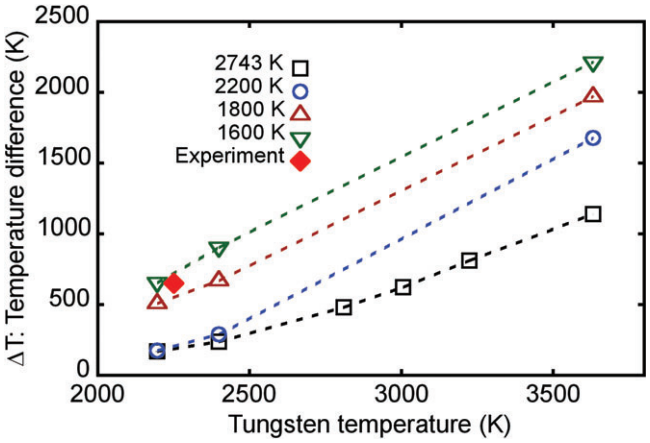

FIGURE 7 Simulation and experimental results of the steady-state back surface temperature. The *x*-axis shows the steady-state back surface temperature of the W specimen. The *y*-axis shows the temperature difference between the W and the Al-coated W specimen for the same irradiation condition. Results with different ablation threshold assumption points were shown

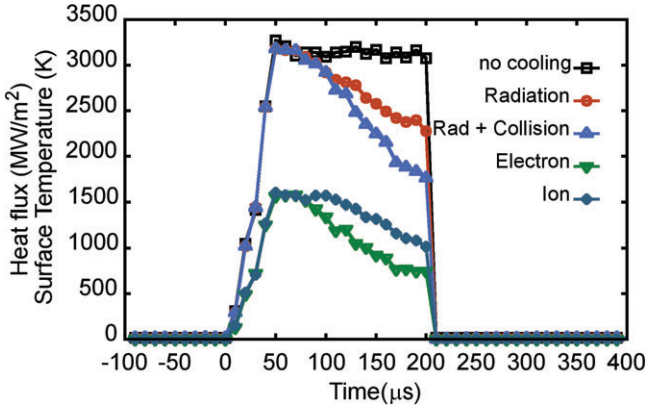

FIGURE 8 Temporal change of heat flux to the Be wall with and without radiation cooling and/or ion–neutral collision models

Thus, it is shown that similar physics can explain the vapour shielding phenomena at PG and reactor. Then, in order to simulate a disruption-relevant condition, higher heat flux calculations are performed by increasing plasma density. In a calculation with $n_e \sim 1 \times 10^{20}$ m^{-3} and q$'' \sim 7$ GW/m^2, oscillating phenomena are observed. As plotted in Figure 9, heat flux, surface temperature, and vapour emission rate are oscillating in a similar fashion. First, the high heat flux heats the surface rapidly. Then, large vapour emission quickly dissipates the incoming plasma flux. The vapour penetrates low-temperature plasma quickly and disappears from the plasma region. Thus, plasma flux can reach the surface again without the energy dissipation by vapour particles. As we test even higher heat flux of up to 14 GW/m^2, increasing oscillating frequency is observed for the higher heat flux as plotted in Figure 10. This increasing frequency is due to the increasing plasma energy dissipation rates. Heat flux drops quickly for higher heat flux cases due to the larger vapour emission; thus, oscillation frequency increases. These oscillating phenomena have been observed in experiments. Pilot-PSI reported oscillating surface temperature of the liquid Sn target.[5] It is also shown that the increasing heat flux from 12.2 to 22 MW/m^2 increases the oscillation frequency. This experimental tendency, higher oscillation at higher heat flux, agrees with the simulation.

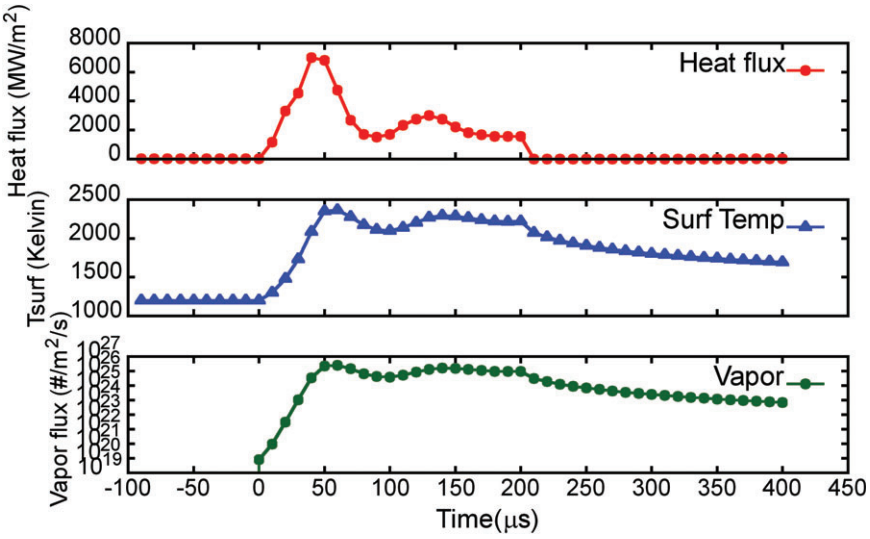

FIGURE 9 Oscillating heat flux, surface temperature, and vapour flux from the surface of the Be wall under the edge-localized mode (ELM)-like heat flux

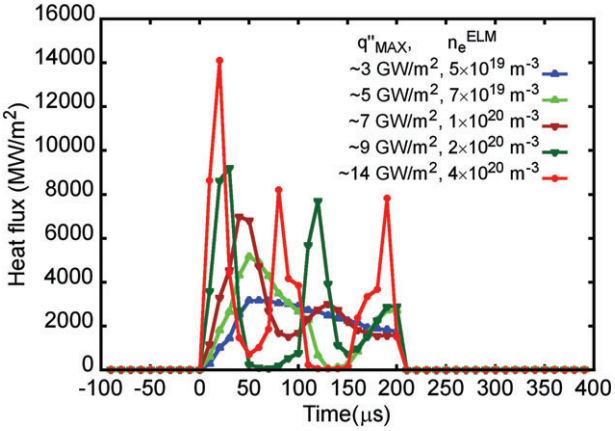

FIGURE 10 Oscillating heat flux for pulses of different maximum heat flux from 3 to 14 GW/m^2

4 | SUMMARY AND FUTURE WORKS

A weighted PIC code, PIXY, is developed for simulations of heat flux dissipation by vapour from a solid wall (vapour shielding). A 1d3v PIC model, including various A&M reactions, is combined with a heat transfer calculation at the wall. The weighted particle method is applied to treat the vapour emission flux, which is largely varied by the wall temperature. The multi-components plasma model reproduces the PG experiment well. The experimental observation of the specimen temperature change for the W and Al-coated W specimens is also reproduced by assuming a lower ablation threshold. Further studies on the ablation threshold and mechanism should be conducted and included in the model. Simulations on the vapour shielding at the transient ELM heat flux for the reactor condition are also performed. It is found that the radiation cooling cannot be the only cooling process during the shielding for both PG and reactor environments. Ion–neutral collision plays an important role in the heat flux dissipation. In the present PIXY, Coulomb collisions and radiation trapping are not taken into account. A collision model for the weighted PIC code [22] and radiation-trapping model will be equipped in the PIXY. In the higher heat flux calculations, the PIXY simulation successfully simulates the oscillation phenomena during the vapour shielding. Further comparison with the experimentally observed oscillations will be considered in the near future.

ACKNOWLEDGMENTS

This work is performed on "Plasma Simulator" (FUJITSU FX100) of NIFS with the support and under the auspices of the NIFS Collaboration Research Program (NIFS16KNXN320). This work is partially supported by the "ZE Research Program, IAE ZE29B-01."

ORCID

K. Ibano http://orcid.org/0000-0001-8171-1928

REFERENCES

[1] J. K. Tripathi, T. J. Novakowski, G. Joseph, J. Linke, A. Hassanein, *J. Nucl. Mater.* **2015**, *464*, 97.
[2] T. Sizyuk, A. Hassanein, *Nucl. Fusion.* **2014**, *54*, 23004.
[3] Y. Kikuchi, I. Sakuma, Y. Kitagawa, Y. Asai, K. Onishi, N. Fukumoto, M. Nagata, Y. Ueda, H. Kurishita, *J. Nucl. Mater.* **2015**, *463*, 206.
[4] G. G. van Eden, T. W. Morgan, D. U. B. Aussems, M. A. van den Berg, K. Bystrov, M. C. M. van de Sanden, *Phys. Rev. Lett.* **2016**, *116*, 135002.
[5] G. G. van Eden, V. Kvon, M. C. M. van de Sanden, T. W. Morgan, *Nat. Commun.* **2017**, *8*, 192.
[6] S. L. Milora, C. A. Foster, *IEEE Trans. Plasma Sci.* **1978**, *6*, 578.
[7] W. A. Houlberg, S. L. Milora, S. E. Attenberger, *Nucl. Fusion.* **1988**, *28*, 595.
[8] Y. Nakamura, H. Nishihara, M. Wakatani, *Nucl. Fusion.* **1986**, *26*, 907.
[9] G. Federici, A. Loarte, G. Strohmayer, *Plasma Phys. Control. Fusion.* **2003**, *45*, 1523.
[10] D. I. Skovorodin, A. A. Pshenov, A. S. Arakcheev, E. A. Eksaeva, E. D. Marenkov, S. I. Krasheninnikov, *Phys. Plasmas.* **2016**, *2*, 22501.
[11] H. Würz, I. Landman, B. Bazylev, F. Kappler, G. Piazza, S. Pestchanyi, *J. Nucl. Mater.* **1996**, *233*, 798.
[12] A. Hassanein, *Fusion Eng. Des.* **2002**, *60*, 527.
[13] K. Ibano, D. Nishijima, J. H. Yu, M. J. Baldwin, R. P. Doerner, T. Takizuka, H. T. Lee, Y. Ueda, *Nucl. Mater. Energy.* **2017**, *12*, 278.
[14] K. Ibano, S. Togo, T. L. Lang, Y. Ogawa, H. T. Lee, Y. Ueda, T. Takizuka, *Contrib. Plasma Phys.* **2016**, *56*, 705.
[15] H. P. Summers, M. G. O'Mullane, AIP Conference Proceedings 1344(2011)179 https://aip.scitation.org/doi/10.1063/1.3585817 **2011**.
[16] A. Hassanein, I. Konkashbaev, *J. Nucl. Mater.* **1999**, *273*, 326.
[17] R. Behrisch, W. Eckstein, *Top. Appl. Phys.* **2007**, *110*, 1.
[18] C. H. Liu, J. G. Wang, R. K. Janev, *J. Phys. B At. Mol. Opt. Phys.* **2010**, *43*, 144006.
[19] P. Schwerdtfeger, Table Exparimental and calcualted static dipole polarizabilities, **2015**. http://ctcp.massey.ac.nz/dipole-polarizabilities (accessed: May 22, 2018).
[20] I. Sakuma, Y. Kikuchi, Y. Kitagawa, Y. Asai, K. Onishi, N. Fukumoto, M. Nagata, *J. Nucl. Mater.* **2015**, *463*, 233.
[21] I. Sakuma, Y. Kikuchi, W. Isono, T. Nakazono, M. Nakane, N. Fukumoto, M. Nagata, *Plasma Fusion Res.* **2015**, *10*, 1205089.
[22] A. Tanaka, K. Ibano, T. Takizuka, H. T. Lee, Y. Ueda, *Contrib. Plasma Phys.* in this issue **2018**.

How to cite this article: Ibano K., Kikuchi Y., Tanaka A., Togo S., Lee H. T., Ueda Y., Takizuka T. Simulation study on the vapour shielding at solid walls under transient heat loads using weighted particle model, *Contributions to Plasma Physics* 2018;58:594–601. https://doi.org/10.1002/ctpp.201700160.